Materials and Design 75 (2015) 47–56

Contents lists available at ScienceDirect

Materials and Design

journal homepage: www.elsevier.com/locate/matdes

Influence of Ti–TiN multilayer PVD-coatings design on residual stresses and adhesion

R. Ali, M. Sebastiani *, E. Bemporad

Roma Tre University, Department of Engineering, Via Della Vasca Navale 79, 00146 Rome, Italy

ARTICLE INFO

Article history:
Received 31 December 2014
Revised 4 March 2015
Accepted 8 March 2015
Available online 9 March 2015

Keywords:
Ti–TiN
Multilayer
Finite element modeling
Residual stress
Optimization

ABSTRACT

Multilayer systems can offer an efficient way of controlling residual stress, improve adhesion and enhance toughness of coated systems. This work aims at the development of multilayer coating with improved adhesion, based on numerical design approach. The numerical model of titanium–titanium nitride (Ti–TiN) multilayer has been formulated with multi-physics FEM, to find the optimal thickness of individual layers in a multilayer that can decrease interfacial axial and in-plane shear stress. These coatings configurations are experimentally produced to quantitatively evaluate the scratch adhesion, in-plane residual stresses, nanoindentation hardness and elastic-modulus. Analytical modeling with FilmDoctor® was performed for accurate adhesion evaluation. The multilayer in comparison with bi-layer shows significant improvement (22%) in adhesion under decreased interfacial stress conditions without any affect on overall coating stiffness and hardness. The multilayer coating in comparison with different configurations was also investigated. Result shows an increase in scratch adhesion of 18% and 27% for the optimal position and thickness of interlayers respectively. Qualitative comparison of in-plane residual stress shows higher stress in bi-layer and lower stress in multilayer with optimal thickness of interlayer. The approach in the study could be used to develop stress-optimized coatings for wear resistance applications.

1. Introduction

Hard-coatings such as titanium nitride (TiN) deposited by physical vapor deposition (PVD) have been widely used as protective coatings due to their excellent mechanical properties. The mechanical and tribological behavior of brittle coatings on compliant substrate materials is very much influenced by in-service loading conditions and residual stresses [1]. To meet the specific functional requirements for various uses, titanium–titanium nitride (Ti–TiN) multilayers in comparison with bi-layer, offer much more ease to control residual stresses, improve adhesion, to increase overall thickness and producing the toughening response.

Hard-coatings failures on relatively compliant substrate in many tribological situations are caused by delamination of coating from the substrate (adhesive failure) and fracture in coating, i.e. cohesive failure [2,3]. The failures are primarily related with relatively high compressive residual stress and stress gradient in coatings. Using a multilayer approach, e.g. by a metal-ceramic combination, could effectively control the residual stress and improve adhesion. An increase in thickness of metallic layer provides a reduction of in-plane stress but could significantly decrease the performance of the multilayer [4]. Alternatively, multilayer configuration having equal thickness of ceramic layers could have different amount of residual stress. In case of comparatively thick TiN ceramic layer a large in-plane residual stress (dense columnar growth at the start is present) near to the substrate, which causes the system's failure due to crack propagation [5]. Therefore, a specific thickness of Ti interlayer is required for a particular TiN coating thickness. The optimum coating layers thickness could further enhance the performance of multilayers in terms of adhesion and toughness. Nonetheless, most of the studies were focused on the characterization of residual stress and only a few on the multilayer coating architecture design [6]. As a result, further development is imperative in the design of stress-optimized multilayer PVD-coatings.

In principle, the interior of ceramic films has equi-biaxial in-plane compressive residual stresses which could cause delamination at edges. In addition, it is well-established that ceramic-coated circular disk-shaped metal components mainly fail by the magnitude of axial stress at or near the radial free edge of the specimen [7]. The associated failure of de-cohesion at metal/ceramic interface resulted in progressive delamination and spallation of coatings. Analytical and finite element models as well as

* Corresponding author.
E-mail address: Marco.sebastiani@uniroma3.it (M. Sebastiani).

http://dx.doi.org/10.1016/j.matdes.2015.03.007
0261-3069/

experimental studies showed the influence of these stress components on coating failures [8–11]. Also, when coating is applied to engineering components with edges corners and relatively rough surfaces generate normal and shear stress at interface. The normal stress across and shear stress along the interface are considered to cause coating delamination as interface has usually lower strength than either of the coating or the substrate. In view of all, the preliminary stress optimization in multilayer represents a compulsory task for practical significance.

In a previous paper [6], the effect of a titanium buffer layer position on the adhesion of TiN based systems has been investigated by finite element modeling and micro-mechanical testing. It was demonstrated [6] that having a lower position of the titanium buffer layer can contribute to improve the adhesion to the substrate. However, a fully automated procedure to find the optimal position of the buffer layer still has to be developed. In addition, the analysis and optimization of systems with the inter-position of the two (or more) titanium layers has not been investigated, yet. In the present work, finite element modeling of residual stress analysis coupled with the ANSYS optimization algorithm was used to design stress-optimized Ti–TiN multilayer configuration comprising of 6-layers.

The objective of current study is two-fold; firstly the finite element modeling based design of Ti–TiN multilayers to find optimal thickness of each layer that could decrease axial stress and secondly, experimental investigation of those multilayer configurations for having their influence on in-plane residual stresses and scratch-adhesion. Finally, the failure modes under scratch adhesion testing are correlated with analytical modeling data and experimentally investigated residual stresses.

2. Modeling activities

2.1. Finite element modeling base design of Ti–TiN multilayer PVD-coatings

Residual stresses in PVD-coatings mainly arise from contribution and interactions of two sources: the thermal stresses and the intrinsic stresses.

Thermal stresses arise from thermal mismatch between coating and the substrate during final cooling from deposition to room temperature. Its effects become exaggerated when multiple layers of materials have different thickness and big difference in stiffness [12]. A thermal mismatch-strain ε_{th}, arises from a change in temperature, and could result in residual stress given by the following equation [13]:

$$\sigma_{th} = \left(\frac{E_f}{1-\nu_f}\right)\cdot\varepsilon_{th} = \left(\frac{E_f}{1-\nu_f}\right)\cdot(\alpha_s-\alpha_f)\cdot(T_{sub\{r\}}-T_{sub\{D\}}) \quad (1)$$

where E_f and ν_f are Young's modulus and Poisson's ratio of the film; $\left(\frac{E_f}{1-\nu_f}\right)$ = bi-axial elastic modulus of the film; α_f and α_s are thermal expansion coefficients of the film and the substrate, respectively; $T_{sub\{r\}}$; $T_{sub\{D\}}$ are the room and deposition temperature of the substrate, respectively. The quantity σ_{th} is the stress that will develop in the thin film. Here, only differential thermal stress is considered; however thermal expansion is structure dependent property which could vary with the layer thickness.

The intrinsic stresses in PVD-coatings arise during deposition and its magnitude depends on deposition conditions, such as reference potential on substrate, pressure of working gas and target to the substrate distance as well as on stoichiometry and thickness of coating layers [14,15].

Usually, the resulting residual stress field is formed by a simple superposition of two sources:

$$\sigma_{tot} = \sigma_i + \sigma_{th} \quad (2)$$

The delamination failure at interface and cohesive failure caused by spallation within multilayer is generally controlled by optimization of this residual stress field. Increase in coating-substrate interfacial adhesion by minimizing residual stress-gradient at interface, will improve the sustainability of interface to the externally imposed shear stress [16].

Possible failure mechanism of progressive coating delamination is caused by de-cohesion at free edges. For this, the relevant axial normal stress (interfacial stress) has been evaluated in the present study; through a sufficiently reliable FEA prediction model and preliminary optimization by adopting realistic simplification hypotheses. Model consists of a circular disk-shape, which exactly reproduced the actual sample shape. The model realized is based on the following simplified assumptions:

1. The interfaces (coating/substrate, multilayer) are assumed to be well-bonded. In the finite element terminology, the nodes are shared at all the interfaces.
2. In order to select an appropriate mesh for a multilayer system, numerical model was validated through numerical tests with different material properties and dimension values of the coating and the substrate [11]. A change in thermal residual stress with a change in thickness was also verified through analytical solution which was achieved by the decrease in bending induced stress with an increase in layer thickness. Finer mesh size at interface was maintained by biasing element size toward coating/substrate interface. While in lower part of the substrate, an increasingly coarse mesh was used in order to decrease the computational time. The thickness of each layer was simulated with sufficient number of elements (number of elements in normal direction) to have stress distribution within each layer.
3. Residual thermal stresses were computed for simulated cooling from an assumed deposition temperature (300 °C) as stress free temperature to room temperature (25 °C) of the substrate.

Residual stress analysis and the optimization algorithm involved iterative solutions: a 2D axi-symmetric model, that represent six layers Ti–TiN multilayer on a stainless steel substrate was developed using ANSYS13 parametric design language (APDL). PLANE 77 element (8-node quadrilateral coupled thermal-structural axisymmetric) was selected for the analysis. Mechanical and thermal properties of materials (Table 1) were assumed as temperature independent and plastic hardening behavior of substrate was taken into account [17]. The bottom left corner of axi-symmetric model was fixed for bending to occur during cooling that changed the residual stress with a change in thickness of the coating layer during the optimization.

In the first step, finite element analysis of residual stress was performed with two models namely; bi-layer and Ti–TiN multilayer system with middle position of interlayers (Fig. 1a). Subsequently, multilayer configuration was optimized in two ways: (i) through changing position of Ti interlayers within fixed

Table 1
Typical physical and thermal properties of coating, interlayer and substrate materials.

Materials	Elastic modulus (GPa)	Poisson's ratio	Thermal expansion (10^{-6} °C^{-1})	Materials behavior
Ti	116	0.32	9.0	Ideal elastic plastic
TiN	600	0.25	9.4	Perfectly elastic
Substrate	200	0.30	13.0	Plastic hardening

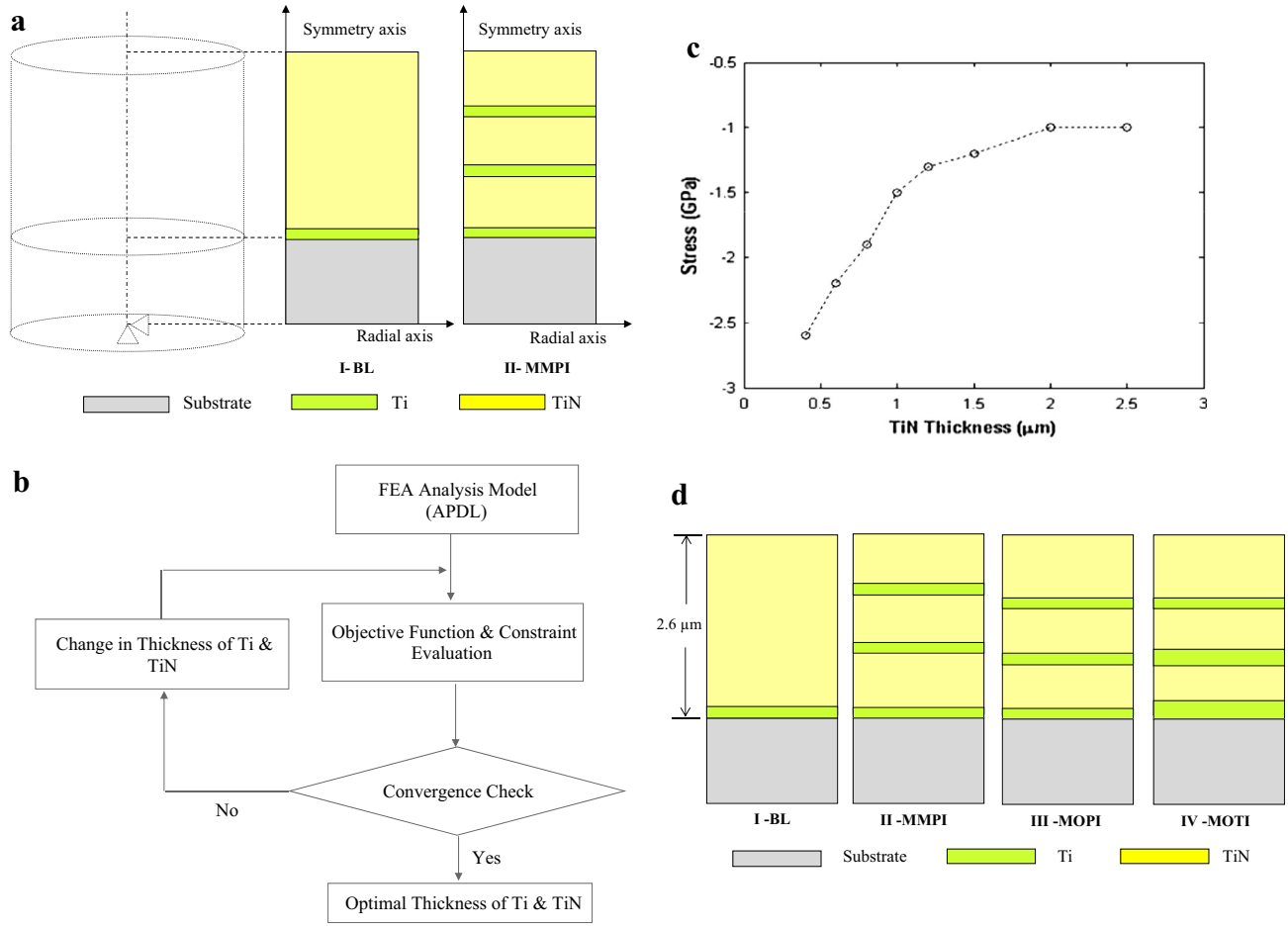

Fig. 1. (a) Schematic description of finite element model realized to evaluate residual stress arising from deposition process, (b) followed optimization frame work, (c) thickness dependent intrinsic stress reproduced in the TiN layers during multilayer optimization, (d) schematic description of multilayer configurations obtained using single objective optimization compared with bi-layer and multilayer configuration with middle position of interlayer.

overall thickness of the three TiN layers, and (ii) with variable thickness of all the Ti interlayers and TiN layers. To facilitate reading, the four models developed are described as follows (thickness of layers always starting from top layer):

i. Model type "BL": Bi-layer (single TiN layer of 2.55 μm thickness and Ti interlayer of 0.05 μm thickness on 300 μm steel substrate);
ii. Model type "MMPI": Multilayer with middle position of Ti interlayers (three TiN layers each of 0.80 μm thickness and three interlayer of Ti each of 0.06 μm thickness on 300 μm steel substrate);
iii. Model type "MOPI": Multilayer with optimal position of Ti interlayers (three TiN layers of thickness 1.10, 0.73 and 0.57 μm, and three interlayers of Ti have equal and similar thickness to model type MMPI);
iv. Model type "MOTI": Multilayer with optimal thickness of Ti interlayers (three TiN layers of 1.10, 0.60 and 0.64 μm thicknesses, and three interlayer of Ti have thickness of 0.06, 0.08 and 0.12 μm).

For a model with fixed number of alternating Ti–TiN layers on the stainless steel substrate, a single-objective constrained (total thickness was constrained during optimization iteration) optimization algorithm (sub-problem) was employed to find the optimal thickness of each coating layer that minimized the axial stress (perpendicular to interface) at the edges. The goal of optimization was to find the best solution for a given problem in design space defined by optimization algorithm. Optimization algorithm contains three components: Design variable (independent variables), constraints (dependent variables) and objective function (dependent variables) to be minimized. Within specified lower and upper limits of design variables and constraints, the optimization algorithm will search in design space for the minimization of objective function with analysis-evaluation-modification cycle as shown in Fig. 1b [18].

Coating layers were used as design variables within constraints of total thickness (2.6 μm). The axial stress at sample edge (normal to surface) was used as objective function. The optimization algorithm will search for minimum objective function within specified upper and lower limits of design and state variables. Thickness of the Ti interlayer varied from 60 to 150 nm. Each TiN layer has initial thickness of 0.8 μm and varied from 500 nm to 1.5 μm.

During optimization, a realistic bi-axial thickness dependent intrinsic stress (ion-peeing stress) in each TiN layer was reproduced as an initial stress using the INISTATE command. It was adopted from growth-stress model for columnar structure [19]. The in-plane intrinsic stress (Fig. 1c) was applied on structural elements of each material and as a check the stress in each solution was written out to a file by issuing the "inis, list" command. In addition, with a change in thickness of TiN during optimization-cycle, the corresponding value of intrinsic stress for that thickness was reproduced on the structural elements and as a monitoring check it was also written out to a file in each previous solution.

All the modeling activities in the present study were carried out on an Intel-Xeon 3 GHz processor machine with 8 GB of random access memory, running a Windows 64-bit operating system and time taken for an optimization was ≈20 min.

Schematic description of the multilayer configurations obtained using single objective optimization (Fig. 1d) in comparison with bi-layer and multilayer configuration with middle position of interlayer.

2.2. Criterion for practical adhesion evaluation and scratch-dimensioning

For practical adhesion evaluation, scratch test is generally used technique in which critical load acting normal to surface at incident of failure is usually related to adhesion between coating and substrate. However, it is strongly affected by various parameters such as scratch indenter tip radius, film thickness, friction effects, hardness and elastic modulus of coatings and substrate material. In hard-coatings cohesive failures are due to an extensive deformation in the compliant substrate by high indenter tip radius during the scratch test. Indenter tip radius significantly controls the depth of deformation zone. The plastic deformation mainly starts in the substrate and does not initiate in coatings until large plastic zone has developed at coating-substrate interface [20]. With relative increase in indenter tip radius, the critical scratch load and deformation depth within substrate is increased. As a result, sufficiently high tensile bending stresses developed in the coating and being sensitive to tensile stress cohesive failure occurs. In general, high compressive shear stress at interface and tensile stress at contact edge cause delamination at interface and crack formation in brittle ceramic layer close to surface [21]. Therefore, the pre-requisite for producing adhesive failures and suppressing cohesive failures in the thin hard coatings on relatively compliant substrate is to choose proper scratch indenter tip radius.

Analytical calculations were performed with analytical modeling software package (FilmDoctor®) to control the position of maximum von-Mises stress (criterion related to the plastic flow of the material due to shear stress) close to interface [22,23]. Maximum von-Mises stress should be increase sufficiently above the critical yield strength of metallic layer at interface to ensure adhesive failure. The state of stress was simulated with tangential frictional force of 10% of the applied normal load (apparent friction coefficient), which roughly model the interaction between indenter and coating. The critical load was determined by scratch test, which is defined as load where delamination or crack failure appears, was used as input to analytical modeling. The interaction was modeled with two hemi-spherical tip conical indenters of tip radii (100 and 200 μm), in order to characterize most likely occurring cohesive and adhesive failures. The position of von-Mises stress with respect to coating-substrate interface and normal stress on the surface at trailing edge of scratch indenter was qualitatively compared. The elastic modulus input data used for analytical modeling were measured with nanoindentation and interaction was modeled without an influence of the coating intrinsic stresses.

3. Experimental details

Starting from results of simulations, three multilayer coating configurations in comparison with bi-layer of Ti–TiN were produced using balanced-magnetron sputtering plant, with DC powered Ti target and RF powered sample holder capable of inducing bias to the substrate. Nitrogen was put into the chamber to produce TiN by reactive sputtering. The coatings were deposited on AISI 304 stainless steel having 25 mm diameter and 5–7 mm thickness. All the substrates were polished to mirror finish, corresponding to R_a values of ≈30–40 nm measured with an optical profilometer. Samples were ultrasonically pre-cleaned in acetone and isopropyl alcohol for 10 min and mounted on a sample holder that was fixed at 110 mm distance from the target. The substrates were subsequently sputter-etched in argon plasma for 10 min in order to remove the surface oxide layer. The chamber was pumped down to a base pressure of 6×10^{-6} mbar and each TiN layer was deposited with 120 and 14 sccm respective flows of argon and nitrogen. The deposition rate of Ti and TiN measured with the Focused Ion Beam (FIB) was ≈1 and 35 nm/min, respectively. The differentiation of each layer thickness was achieved by choosing the deposition time. All the TiN layers were coated with an applied potential of 150 V while all the Ti layers were coated with floating potential (≈30 V from plasma). The substrate temperature developed during the deposition and ion-etching was measured with a temperature measurement strip gauge. The gauges were mounted on the rod which held the sample on the other side. The measured temperature at the end of deposition was 290 °C.

After deposition, the morphological characterization including individual layer thickness and presence of columnar structure was examined using the FIB.

Intrinsic hardness and reduced modulus of bi-layer and three multilayer configurations were measured by nanoindentation (Nano Indenter Agilent G-200). A diamond Berkovich indenter was used to perform the measurements in continuous stiffness measurement mode. The correct load-displacement curves were analyzed with the classical Oliver and Pharr [24,25] procedure, and hardness and elastic modulus were evaluated as an average of sixteen measurements. Mechanical properties were evaluated for penetration depth within 10% of the coating thickness to avoid substrate effects.

The scratch tests were performed on bi-layer and three multilayer configurations in order to evaluate adhesion to the stainless steel substrate. According to the UNI EN 1071 (3) standard at least three scratches are to be performed on each sample with a CSM Instruments Revetest [26]. A 10 mm long scratch was made using the Rockwell "C" diamond indenter tips of radii 100 and 200 μm with sliding speed of 10 mm/min and loading rate of 30 N/min. A progressively increasing loading mode with starting load of 1 N was used to identify the start of scratch track. Adhesion was quantitatively evaluated (critical loads: L_{C1}; the first delamination (partial appearance of substrate); L_{C2}; complete delamination (semicircular appearance of substrate)) by means of scratch data analysis. After scratch, the critical load for failure was calculated by analyzing the scratch track using optical profilometer.

The in-plane residual stresses analysis in the bi-layer and three multilayer configurations were conducted with Bruker D8 Discover System in parallel beam geometry optics arrangement using Cu-Kα radiation. The precision of residual stress measurement with classical X-ray $\sin^2\psi$ depends strongly on accurate determination of diffraction peak position. Several full scans in the Bragg-Brentano (θ-2θ scan mode) were performed to identify the peak at high angle to be used for residual stress quantification. The TiN (1 1 1) peak shifted with reference to the standard TiN powder diffraction data which shows that coatings were (under or over) stoichiometric [27]. Moreover, the lower angle peak (1 1 1) was intense and higher angle peaks were very weak. Therefore, X-ray data were collected for the peaks (4 2 2) and (5 1 1) for all samples at grazing-incidence X-ray diffraction (GIXRD) for qualitative residual stress analysis. The grazing angle was set at 1° for all the coatings with a scan step size of 0.02° over a 2θ range of 110–160°. The grazing-incident is reasonable to have residual stress from a shallow region of coatings for qualitatively comparison.

4. Results

4.1. Modeling results

4.1.1. Finite element modeling base design of Ti–TiN multilayer PVD-coatings

The analysis was first performed to assess the independent effect of thermal stress and validate the in-plane stress with analytical solutions. Elastic theoretical calculations showed good agreement with FEM solution [28]. Then combined effects of thermal and intrinsic stress on axial stress profile were examined. The axial stress along the node path in corresponding to model edge for bi-layer and multilayers is presented in Fig. 2. As expected, high in-plane stress coupled with normal to surface stress shows a peak in TiN layer adjacent to substrate and obviously is zero at the free surface. Qualitative comparison of axial stress component (Fig. 2a) in multilayer coating configuration (MMPI) with bi-layer (BL) shows a difference of ≈16%. The introduction of two Ti interlayers shows significant decrease in interfacial axial stress.

Further, based on axial stress profile in multilayer configuration (MMPI) as shown in Fig. 2a, being not symmetric as maximum magnitude is in TiN layer close to the substrate; two types of optimization were performed. During the first optimization, only the thickness of all the TiN layers were changed within fixed Ti interlayer thickness; this only change the position of Ti interlayer compared with the middle position of interlayer multilayer configuration (MMPI). While during the second optimization, thickness of all the layers was changed within the fixed final thickness.

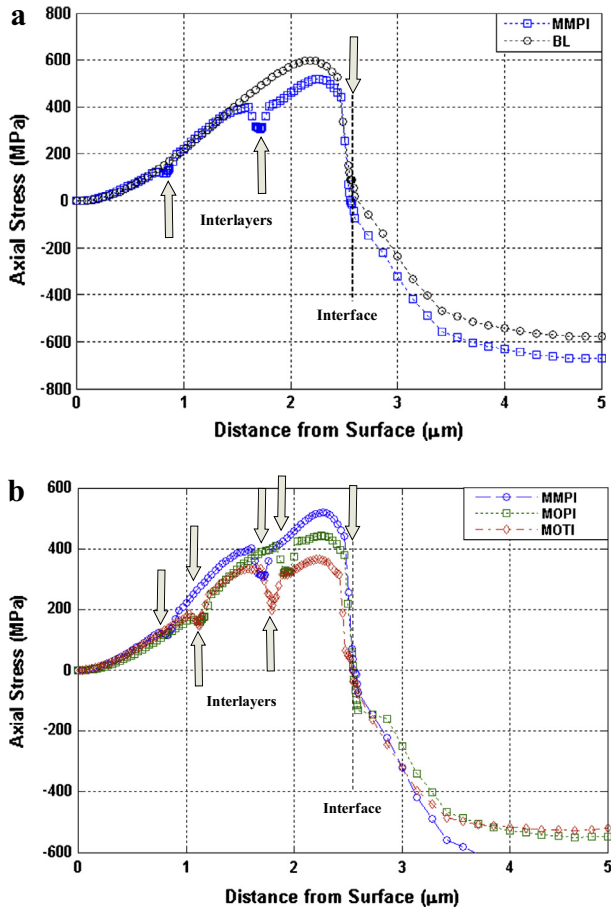

Fig. 2. Qualitative comparison of predicted normal to surface stress: (a) stress profile in model BL in comparison with model MMPI, (b) stress profile in two models of multilayer configurations, MOPI and MOTI compared with model MMPI.

By changing the position of Ti interlayers (first optimal configuration), a significant decrease in the interfacial axial stress was observed as shown in Fig. 2b. The decrease in stress was ≈10% compared with multilayer configuration in which all the TiN layers have equal thickness; however, it is significantly decreased in comparison with bi-layer. In case of the second optimal configuration in which thickness of both Ti and TiN layers were changed, a decrease of ≈25% in the axial stress was observed with an increase of ≈4% relative quantity of Ti in the multilayer. With further increase in Ti interlayer thickness and decrease in the TiN layer thickness within specified final thickness, thickness dependent residual stress involved that limit the optimization and also it is practicably unacceptable.

In-plane shear stress in the bi-layer and multilayer configurations was far less than other stress components along the same path. Maximum shear stress was at interface between TiN and Ti interlayer close to the substrate and peak of maximum slightly shifted toward the Ti interlayer which could affect adhesion adversely.

4.1.2. Criterion for practical adhesion evaluation and scratch-dimensioning

The critical failure load was determined with real scratch test and correlated to the simulated stress field to characterize the failure mode (adhesive and cohesive). It was found that indenter with tip radius of 100 μm was suitable to produce the adhesive failure. For the large radii indenter (200 μm), cracking and chipping was the predominant observed failure mode. As the critical scratch load increased for larger indenter tip radius, the resulting failures were cracks beyond scratch edges (cohesive failures). The position of the maximum von-Mises stress at critical failure load was shifted deep into the substrate and probably most of the load was used to produce deformation in substrate. As a result, sufficiently high bending induced tensile stresses on the sides of the scratch track reached critical cohesive strength of TiN which perhaps caused failure. However, critical failure load with a smaller indenter tip radius (100 μm) was found lower and plastic flow increased and shifted to the substrate surface region. As shown in Fig. 3a wherein, the interface is indicated by white dash line and black dot marks the position of the maximum von-Mises stress.

In case of multilayer, critical scratch load was sufficiently higher even with 100 μm indenter tip radius, for which the maximum von-Mises stress shifted more deep into the substrate. However, the von-Mises stress close to interface was significantly high enough to cause the delamination. This indicates relatively higher adhesion of multilayers compared with the bi-layer. In view of the analytical analysis, it was found that shallow position of maximum von-Mises stress was responsible for adhesive failure.

4.2. Experimental results

4.2.1. Morphological characterization of coatings

After deposition, the thickness of individual layer in multilayer and presence of Ti interlayer was observed with the focus ion beam (FIB) cross-section measurements. The images are shown in Fig. 4. The sample MOTI (multilayer with optimal thickness of interlayer) shows slightly less overall thickness. Individual TiN layers and Ti interlayer thickness were within the range of ±50 nm and ±10 nm, respectively. All the samples show columnar growth in all the TiN layers. However, layer close to the substrate shows dense growth of columns which could result in relatively high stress in the layer.

4.2.2. In-plane residual stress analysis

For qualitative comparison of in-plane residual stress in bi-layer and multilayer configurations, the grazing-incidence X-ray

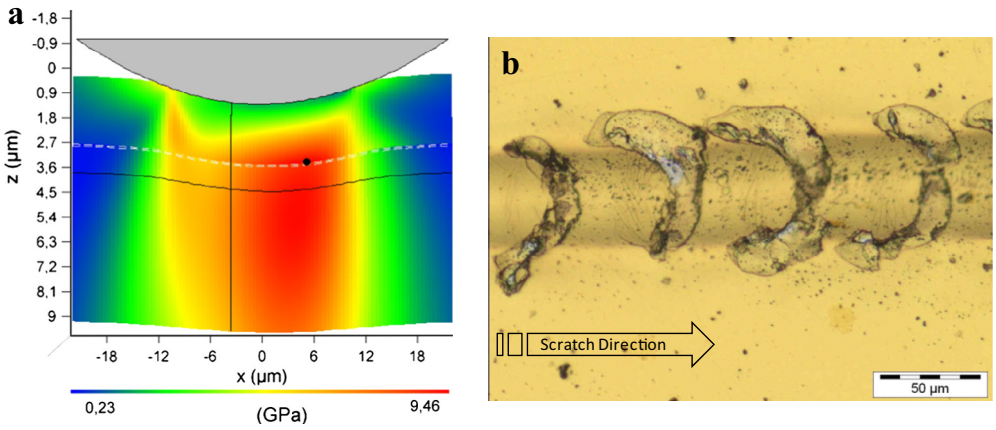

Fig. 3. (a) Position of von-Mises stress at the moment of observed critical scratch load (L_{C1}) in bi-layer coating, (b) corresponding failure in bi-layer at incident of critical scratch load with 100 µm indenter.

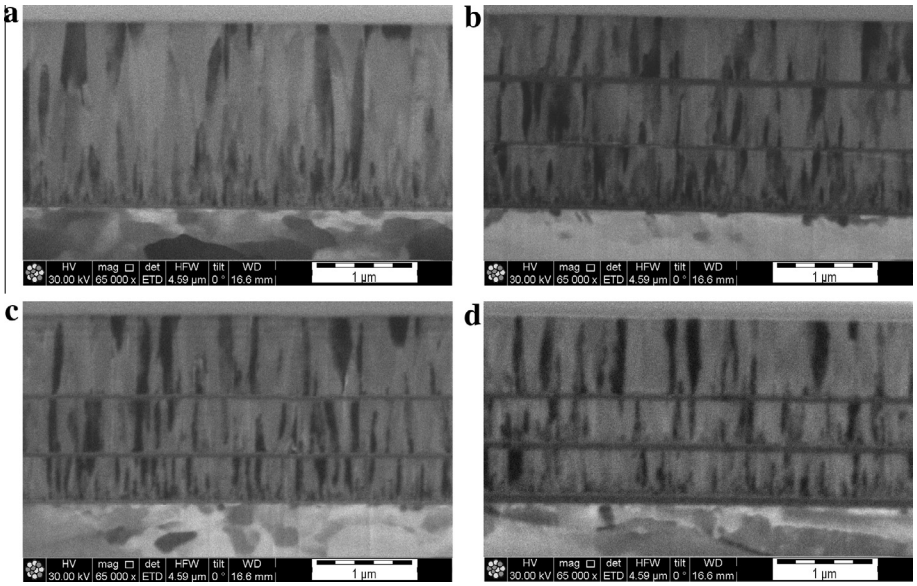

Fig. 4. The FIB cross-section observation (30 kV, ETD, 65,000× in all the cases): (a) sample BL, (b) sample MMPI, (c) sample MOPI, (d) sample MOTI. Columnar structure and presence of Ti layer is clearly visible.

diffractogram are shown in Fig. 5. The diffraction patterns were smooth and shifted vertically for clarity. It was assumed that all the coatings were in compressive residual stress. The difference in peak position of bi-layer and multilayer coating configurations diffractogram is primarily due to difference in residual stress. Considering X-ray diffractogram analysis, the high angle diffraction peak (5 1 1) in bi-layer is shifted to lower 2θ angle compared with multilayer sample MMPI which showed that BL sample has higher residual stress. The multilayer samples MMPI and MOPI almost have similar peak position and MOTI diffractogram shifted toward high angle showing lower residual stress among all the multilayer configurations.

4.2.3. Nanoindentation

The results of indentation test in bi-layer and different multilayer configurations are presented in Fig. 6. An increase in hardness for shallow displacement might result from surface roughness. For penetration depth of 100 nm multilayer configuration shows slightly higher hardness than that of bi-layer but it remained within the limits of standard deviation. By taking penetration depth of 150 nm (penetration depth less than one-tenth of coating thickness) multilayer with middle position of interlayer slightly decrease its hardness compare to other configurations. The difference in hardness between the remaining two multilayer configurations appears clearly due to Ti quantity. The nanoindentation modulus for coating configurations is shown in Fig. 6b. The values are derived from the continuous stiffness measurements. The effective modulus values of multilayers decreased with increasing displacement into coated system. The hardness and modulus are more stabilized at penetration depth of 100 nm.

4.2.4. Scratch adhesion

The scratch tracks in coatings were observed with an optical profilometer and images at incident of the first failure (L_{C1}) are shown in Fig. 7. The first failure in all the coating configurations was semi-circular cracks due to buckling inside the scratch track accompanied with the first delamination within the track. It is commonly occurring failure in hard coating on compliant substrate like stainless steel [29]. The amount of spallation is high and continued until final delamination in the bi-layer. However in the multilayer, it occurs with intermediate conformal cracking. It seems that thicker ceramic layer of TiN in bi-layer is responsible for

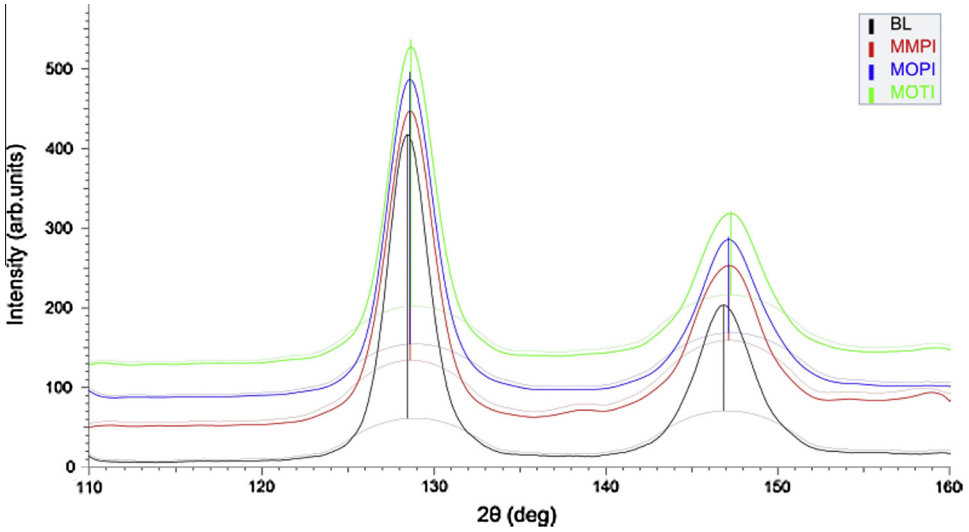

Fig. 5. X-ray diffractogram at grazing incidence of the bi-layer and multilayer configurations.

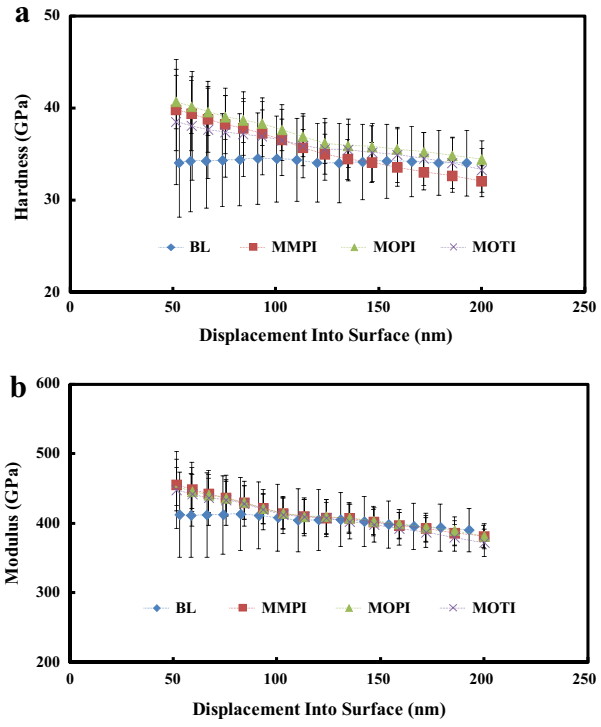

Fig. 6. Intrinsic hardness and elastic modulus in bi-layer and multilayer configurations.

continuous spallation of coating at relatively lower critical scratch load as shown in Fig. 7a where the white region in track is the substrate. As the multilayer configurations with ductile interlayers absorbed more energy, consequently spallation took place at significantly high critical scratch load.

The adhesion of coatings in relation to critical adhesive load at incident of failure is shown in Fig. 9. An enhancement in the first and second critical adhesive loads of multilayer was found to be 50% and 22%, respectively in relation to bi-layer. When multilayer was compared with different configurations, an optimal position of the interlayer and optimal thickness of interlayer showed improvement by 16% for the L_{C1}, and 18% and 27%, respectively for the L_{C2}.

5. Discussion

Finite element results show that axial stress at radial free edge plays a major role in the optimization of Ti and TiN thickness in multilayer configurations. The decrease in stress is much effective in case of model MOPI (Fig. 2b). However in case of model MOTI, an increase in thickness of intermediate Ti interlayer and interlayer between coating-substrate interface lead to a much more effective decrease in stress peak by elastic deformation of less stiff Ti layers while Ti interlayer close to top surface remained ineffective. It was found that axial stress was distributed similarly in all the configurations (bi-layer and multilayer), but the peak value of stress varied from one configuration to another. The peak value is significant to enhance crack propagation from the edge, along the interface or within the TiN close to the interface [30]. Scratch adhesion results confirmed that interlayer thickness-optimized multilayer (sample MOTI) involved remarkable increase in adhesion; the critical adhesive load L_{C2} measured for this multilayer configuration was found to be 27% higher than obtained for the multilayer with middle position of interlayer (sample MMPI).

The optimization of multilayer configurations involved a decrease in only the axial stress component at the edge of model. As a result, it was possible that other stress components such as in-plane shear and in-plane residual stress might increase. Therefore, as a monitoring check, in-plane shear stress was analyzed during the finite element calculations along the same path and in-plane residual stress was experimentally investigated with X-ray diffraction in the produced multilayer coating configurations.

The difference in in-plane shear stress component among the multilayer configurations is not very significant as maximum shear stress was far less than other stress components. Even though this stress component is small it decreased the possible initiation of spallation at the edge. Although modeling approach and materials behavior significantly differed with the actual multilayers but generally these changes may be beneficial for suppressing the crack propagation and improving the adhesion.

Considering X-ray diffractogram analysis, the bi-layer (sample BL) has the highest in-plane residual stress among all the multilayer configurations (samples MMPI, MOPI and MOTI). The introduction of two interlayers significantly controls the residual stress and improves the critical adhesive load. In addition, the FIB cross-section analysis reported in Fig. 4 showed columnar growth structure of PVD TiN layers which terminated with Ti

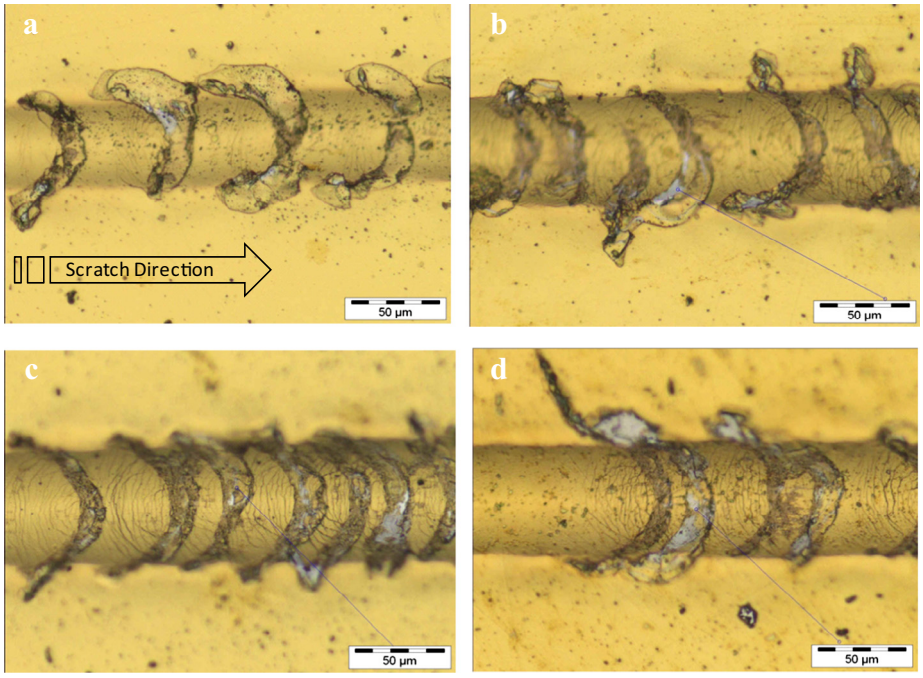

Fig. 7. The first delamination failure (partial appearance of substrate) in bi-layer and multilayers: (a) sample BL, (b) sample MMPI, (c) sample MOPI, (d) sample MOTI.

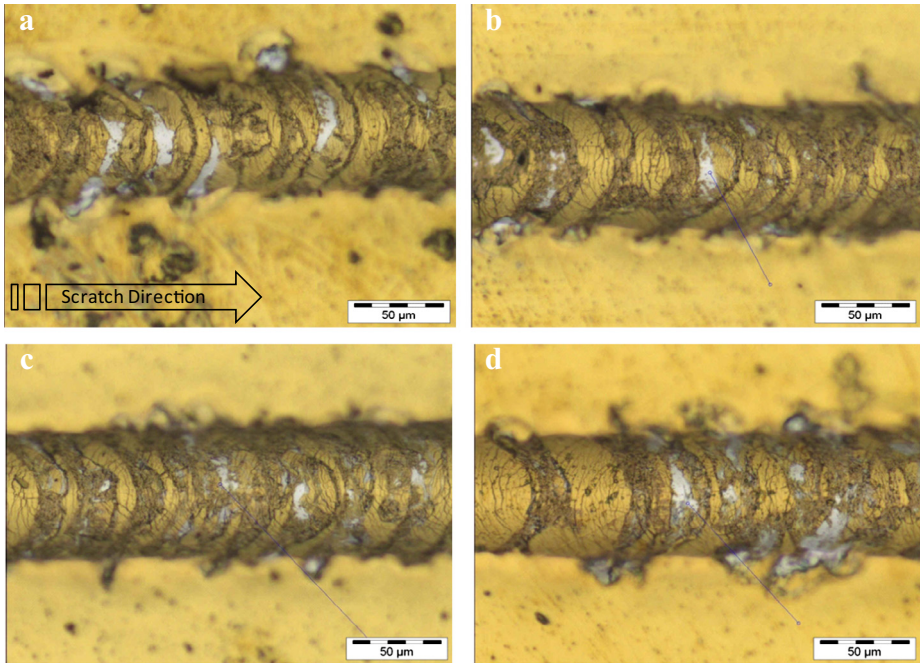

Fig. 8. Complete delamination failure (semicircular appearance of substrate) in bi-layer and multilayers: (a) sample BL, (b) sample MMPI, (c) sample MOPI, (d) sample MOTI.

interlayer in the multilayer configurations. This could be one of the main reasons of decreased residual stress and improved adhesion of multilayer configurations. Stress analysis in individual TiN layer of multilayer system is of considerable greater scientific and technological importance for multilayer development. The work is on-going with the micro-scale FIB-DIC ring core [31] and more advanced XRD techniques.

The analytical modeling for scratch dimensioning with different indenter radii demonstrated the possibility to adjust the depth of maximum von-Mises at coating-substrate interface to induce adhesive failure. As shown in Fig. 3b, high tensile stress at surface in combination with weakening of interface by plastic flow at interface caused severe shearing off the bigger coating areas [32]. The simulated von-Mises stress with an indenter tip radius of 100 μm and corresponding adhesive failure at the first critical scratch load is shown in Fig. 3. It shows good agreement between the analytical and experimental results of virtual and real scratch tests. In addition, results indicate the significance of analytical measures to produce adhesive failure and suppress cohesive failure.

Besides spallation within scratch track, Figs. 7 and 8 show fine tensile cracks (semicircular crack parallel to trailing edge of

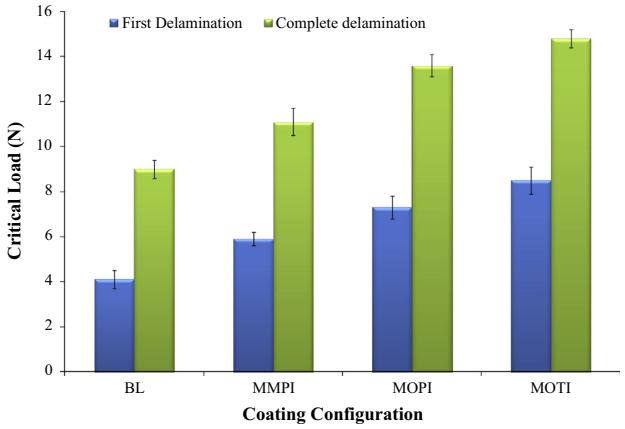

Fig. 9. Critical scratch load for the first failure (L_{C1}) and complete failure (L_{C2}) in the bi-layer and multilayers.

indenter) on the site of buckling failure which are predominant in multilayer configurations that reflect coating still adhered to the substrate. These cracks occur as a result of equilibrium between tensile frictional forces on trailing edge of indenter with compressive frictional force ahead of indenter [21]. This could be due to high friction stress involved by the presence of Ti interlayer with the indenter [33]. Also, it could be expected that critical load in multilayer might be affected by the friction between Ti and diamond indenter. Specifically, the multilayer MOTI configuration showed the smearing of Ti along the scratch track due to its high adhesion.

In one of authors previous work [6], a four-layers Ti–TiN multilayer coating were numerically analyzed and experimentally tested. In that work, only three Ti–TiN multilayer (four layers) configurations showed significant improvement in adhesion, toughness and hardness, when a Ti buffer layer was placed in lower position of the coating thickness. In the present work, which is an extension of the previous work [6] robustness was provided using ANSYS optimization algorithm to use it for Ti and TiN thickness optimization and reproducing the realistic residual stress during the optimization. The results suggested the significance of optimization measures to develop stress-optimized multilayer for improved adhesion.

6. Conclusions

The design and optimization of the Ti–TiN multilayer PVD-coating thickness were performed by finite element analysis to minimize the interfacial axial and shear stress produced under the influence of thermal and intrinsic stresses. Considering the experimental results of scratch adhesion, it was found that multilayer compared with the bi-layer showed significant improvement (22%) in the critical load. With an introduction of two interlayers, the stiffness and hardness of composite multilayer remained the same as recorded in nanoindentation results. The multilayer with optimal position of interlayer showed improvement by 18% and the best configuration with optimal thickness of interlayer showed 27% increase in the critical adhesive load.

The results of virtual scratch test provided comprehensive interpretation of observed failure and demonstrated its importance in order to accurately estimate specific coating properties such as practical adhesion.

Concerning the in-plane XRD-residual stress analysis, the multilayer with optimal interlayer thickness has lower residual stresses and bi-layer has higher stress. To develop an improved understanding in stress-optimized multilayer coating design residual stress in individual coating layer perhaps will be required.

Acknowledgements

This work has received research funding from the European Union, within the large collaborative project ISTRESS, Grant Agreement No. 604646. The authors would like to thanks Daniele de Felicis for his cooperation in FIB cross-sections and Andrea D'Abronzo for his assistance in the production of coatings and Marco Renzelli for XRD measurements. All the modeling and characterization activities were carried out at the "Inter-Departmental Laboratory of Electron Microscopy" (LIME), University ROMA TRE (http://www.lime.uniroma3.it).

References

[1] J. Lackner, L. Major, M. Kot, Microscale interpretation of tribological phenomena in Ti/TiN soft-hard multilayer coatings on soft austenite steel substrates, Bull. Pol. Acad. Sci.: Techn. Sci. 59 (2011) 343–355.
[2] H. Djabella, R. Arnell, Finite element comparative study of elastic stresses in single, double layer and multilayered coated systems, Thin Solid Films 235 (1993) 156–162.
[3] H. Hintermann, Adhesion, friction and wear of thin hard coatings, Wear 100 (1984) 381–397.
[4] G. Kim, S. Lee, J. Hahn, B. Lee, J. Han, J. Lee, et al., Effects of the thickness of Ti buffer layer on the mechanical properties of TiN coatings, Surf. Coat. Technol. 171 (2002) 83–90.
[5] L. Wang, X. Zhong, Y. Zhao, S. Tao, W. Zhang, Y. Wang, et al., Design and optimization of coating structure for the thermal barrier coatings fabricated by atmospheric plasma spraying via finite element method, J. Asian Ceram. Soc. 2 (2014) 102–116.
[6] E. Bemporad, M. Sebastiani, F. Casadei, F. Carassiti, Modelling, production and characterisation of duplex coatings (HVOF and PVD) on Ti–6Al–4V substrate for specific mechanical applications, Surf. Coat. Technol. 201 (2007) 7652–7662.
[7] M. Grujicic, H. Zhao, Optimization of 316 stainless steel/alumina functionally graded material for reduction of damage induced by thermal residual stresses, Mater. Sci. Eng., A 252 (1998) 117–132.
[8] V. Teixeira, Mechanical integrity in PVD coatings due to the presence of residual stresses, Thin Solid Films 392 (2001) 276–281.
[9] U. Wiklund, J. Gunnars, S. Hogmark, Influence of residual stresses on fracture and delamination of thin hard coatings, Wear 232 (1999) 262–269.
[10] J. Wright, R. Williamson, K. Maggs, Finite element analysis of the effectiveness of interlayers in reducing thermal residual stresses in diamond films, Mater. Sci. Eng., A 187 (1994) 87–96.
[11] X. Zhang, B. Xu, H. Wang, Y. Wu, Analyses of interfacial stresses and normal stresses within an elongated film strip/substrate system, Thin Solid Films 515 (2006) 2251–2256.
[12] H. Bhadeshia, Developments in martensitic and bainitic steels: role of the shape deformation, Mater. Sci. Eng., A 378 (2004) 34–39.
[13] Y. Pauleau, Generation and evolution of residual stresses in physical vapour-deposited thin films, Vacuum 61 (2001) 175–181.
[14] P.H. Mayrhofer, M. Geier, C. Löcker, L. Chen, Influence of deposition conditions on texture development and mechanical properties of TiN coatings, Int. J. Mater. Res. 100 (2009) 1052–1058.
[15] J.A. Thornton, D. Hoffman, Stress-related effects in thin films, Thin Solid Films 171 (1989) 5–31.
[16] J. Gerth, M. Larsson, U. Wiklund, F. Riddar, S. Hogmark, On the wear of PVD-coated HSS hobs in dry gear cutting, Wear 266 (2009) 444–452.
[17] W. Smith, J. Hashemi, Foundations of Materials Science and Engineering, McGraw-Hill, 2006.
[18] I. Ansys, ANSYS advanced analysis techniques guide, Ansys Help (2007).
[19] R. Daniel, K. Martinschitz, J. Keckes, C. Mitterer, The origin of stresses in magnetron-sputtered thin films with zone T structures, Acta Mater. 58 (2010) 2621–2633.
[20] Y. Sun, A. Bloyce, T. Bell, Finite element analysis of plastic deformation of various TiN coating/substrate systems under normal contact with a rigid sphere, Thin Solid Films 271 (1995) 122–131.
[21] P. Burnett, D. Rickerby, The scratch adhesion test: an elastic–plastic indentation analysis, Thin Solid Films 157 (1988) 233–254.
[22] N. Schwarzer, Q.-H. Duong, N. Bierwisch, G. Favaro, M. Fuchs, P. Kempe, et al., Optimization of the scratch test for specific coating designs, Surf. Coat. Technol. 206 (2011) 1327–1335.
[23] FilmDoctor®: Software package, <www.siomec.de/FilmDoctor>.
[24] W.C. Oliver, G.M. Pharr, An improved technique for determining hardness and elastic modulus using load and displacement sensing indentation experiments, J. Mater. Res. 7 (1992) 1564–1583.
[25] W.C. Oliver, G.M. Pharr, Measurement of hardness and elastic modulus by instrumented indentation: advances in understanding and refinements to methodology, J. Mater. Res. 19 (2004) 3–20.

[26] STANDARD B. Advanced technical ceramics—methods of test for ceramic coatings, 2003.
[27] M. Leoni, P. Scardi, S. Rossi, L. Fedrizzi, Y. Massiani, (Ti, Cr) N and Ti/TiN PVD coatings on 304 stainless steel substrates: texture and residual stress, Thin Solid Films 345 (1999) 263–269.
[28] C. Hsueh, A. Evans, Residual stresses in meta/ceramic bonded strips, J. Am. Ceram. Soc. 68 (1985) 241–248.
[29] S. Bull, Failure mode maps in the thin film scratch adhesion test, Tribol. Int. 30 (1997) 491–498.
[30] J. Drake, R. Williamson, B. Rabin, Finite element analysis of thermal residual stresses at graded ceramic–metal interfaces. Part II. Interface optimization for residual stress reduction, J. Appl. Phys. 74 (1993) 1321–1326.
[31] A.M. Korsunsky, M. Sebastiani, E. Bemporad, Focused ion beam ring drilling for residual stress evaluation, Mater. Lett. 63 (2009) 1961–1963.
[32] T. Chudoba, N. Schwarzer, F. Richter, New possibilities of mechanical surface characterization with spherical indenters by comparison of experimental and theoretical results, Thin Solid Films 355 (1999) 284–289.
[33] S. Bull, D. Rickerby, A. Matthews, A. Leyland, A. Pace, J. Valli, The use of scratch adhesion testing for the determination of interfacial adhesion: the importance of frictional drag, Surf. Coat. Technol. 36 (1988) 503–517.